IEEE Access
Multidisciplinary | Rapid Review | Open Access Journal

Received 13 November 2022, accepted 3 January 2023, date of publication 10 January 2023, date of current version 13 January 2023.

Digital Object Identifier 10.1109/ACCESS.2023.3235728

RESEARCH ARTICLE

Investigation on the Surface Condition of Gamma Irradiated Silicone Rubber Micro-Nanocomposites

J. MANOJ DHIVAKAR[1], MYNENI SUKESH BABU[1], RAMANUJAM SARATHI[1], (Senior Member, IEEE), STEFAN KORNHUBER[2], AND NARESH CHILLU[3], (Member, IEEE)

[1]Department of Electrical Engineering, IIT Madras, Chennai 600036, India
[2]Department of High Voltage Engineering, University of Applied Sciences Zittau/Görlitz, 02763 Zittau, Germany
[3]School of Electronics Engineering, VIT-AP University, Amaravati, Andhra Pradesh 522237, India

Corresponding author: Naresh Chillu (naresh.ch@vitap.ac.in)

ABSTRACT Silicone rubber (SR) micro nanocomposites formed with micro-ATH and nano-alumina particles have been subjected to different levels of gamma-ray irradiation to understand the characteristic variation in the surface condition of the material through contact angle measurement, Atomic Force Microscopy (AFM) studies, water droplet-initiated corona inception voltage (CIV) measurement and by laser-induced breakdown spectroscopy (LIBS) analysis. It is realized that the recovery rate of silicone rubber micro nanocomposites is less compared with the base SR material. It is observed that, irrespective of the level of irradiation, the contact angle and water droplet initiated CIV of the specimen have shown direct correlation. FTIR analysis clearly indicates variation in methyl group formation on irradiation is less with S2 specimen. It is also observed that fractal dimension calculated by three different techniques for the surface profile data obtained using AFM is in directly in proportion with average surface roughness. In addition, the lacunarity values of the irradiated samples followed the same pattern as that of the average surface roughness. The variation in thermal degradation temperature has been analyzed by adopting thermogravimetric analysis (TGA). The calculated plasma temperature values from laser-induced breakdown spectroscopy and the crater depth formed due to laser ablation have shown inverse relationship. Artificial neural network (ANN) has been employed successfully using LIBS data, to understand the level of irradiation of the SR samples. Overall, the silicone rubber micro-nanocomposite sample S2 filled with micro-ATH and nano Alumina has reflected relatively lesser degradation after being exposed to gamma irradiation, over other test specimens.

INDEX TERMS Silicone rubber, nano-ATH, alumina, AFM, LIBS, TGA.

I. INTRODUCTION

Silicone rubber insulators are becoming popular to use in the power system network, due to their light weight, resistance to vandalism and high surface hydrophobic properties. In recent literature, various researchers have indicated that the addition of inorganic fillers to the silicone rubber base material have improved the electrical, mechanical, thermal and chemical properties [1], [2]. Meyer et al. have reported that the addition of 30 to 50 wt% ATH micro fillers imparted good tracking and erosion resistance to SR material by reducing the effect of temperature during arcing [3]. Also, it is mentioned that the reinforcement of Alumina nano particles improves the dielectric behavior along with erosion resistance of the SR nanocomposite material [4]. The micro-cracks formation due to exposure of corona discharges has been reduced by the incorporation of SiO_2 nanoparticles into base SR material [5]. Recent literature showed that the co-addition of micro-ATH and alumina nanoparticles significantly improved the resistance against AC corona discharges [6].

In case of polymeric insulating materials, the impact of ambient conditions plays a vital role. Especially, at nuclear

The associate editor coordinating the review of this manuscript and approving it for publication was Shuihua Wang.

power plants, where the long-term reliability of electrical equipment is crucial, the properties of polymeric insulating material should not deteriorate easily, after being exposed to radiations. Silicone rubber forms an important insulating material, specifically for cables in nuclear power plants. SR exhibits greater thermal stability and high electrical resistance because it is made up of siloxane bonds (Si-O-Si) with a higher binding energy than C-C bonds, which is present in organic polymers [7].

Especially in space research, many satellite and spacecraft systems and subsystems are vulnerable to radiation from ambient space conditions and onboard sources. Silicone rubber is one of the materials used extensively in nuclear power plants and satellite systems [7], [8]. The radiation exposure can potentially degrade the properties of the spacecraft material which can endanger the proper functioning of the spacecraft. Radiation resistance of employed materials plays a vital role in deciding the space system functionality and satellite lifespan [8]. Polymeric composite materials are the intriguing alternatives to lead and concrete in radiation shielding because to its lightweight, flexibility, durability and superior electrical, mechanical and radiation resistance qualities [9], [10]. Another crucial factor which can affect the functioning spacecraft and its electronic equipment is the electrostatic charging of the spacecraft surfaces [11], [12].

High-energy photons like gamma rays can transfer their energy to materials via photoelectric processes including electron-hole pair production and Compton scattering. Free radicals are produced when gamma ray energy is absorbed by an organic polymer and these radicals react with oxygen in the presence of oxygen to produce peroxy radicals and hydroperoxides. Which further interact with polymer molecules leading to the occurrence of crosslinking and chain scission reactions in the polymer [13], [14], [15]. The impact of gamma radiation on the polymeric insulating materials is mainly dependent on the radiation dosage as well as ambience of irradiation [16]. Due to the degradation phenomenon like oxidation and chain scission, the molecular structure of the polymeric material gets altered and leads to the brittle fracture of the material [17]. Also, the literature regarding the impact of gamma irradiation on the surface recovery characteristics of SR micro-nanocomposites is scanty. Hence, an attempt has been made in the present work to understand the surface recovery properties of gamma irradiated silicone rubber composites formed with micro-ATH and nano-alumina particles.

Tokoro et al observed a significant variation in hydrophobicity loss and recovery characteristics of SR samples after corona ageing by measuring contact angle on its surface [18]. András et al stated that, after the exposure of SR material to corona discharge, the complete recovery was not observed due to the oxidation on the surface of SR [19]. Recently, the variation in the surface morphology of SR after corona ageing has been investigated by performing 3D surface profile analysis, by using AFM technique [20]. Thus, the hydrophobicity and surface profile variation of SR micro-nano composites due to gamma ray-irradiation have been investigated in the present work by adopting static contact angle and AFM technique.

Calculating the fractal dimension, with the 3D image profiles gives the statistical measure of complexity of the surfaces. It can help in understanding the morphological changes in test specimens. Reports have shown various methods for the determination the fractal dimension of the different surfaces [21], [22], [23]. Huang et al. [24] examined the performance of the box counting and variation approaches on Takagi and Brownian motion curves while highlighting the importance of resolution and quantization as constraints on the estimate process. Hence, an attempt has been made in present study to determine the fractal dimension using various techniques.

Laser Induced Breakdown Spectroscopy (LIBS) is a useful and non-destructive technique to identify the elements present in the material. LIBS analysis is also helpful to understand the variation in the surface properties of the material through the calculation of plasma temperature and electron density calculation [25], [26]. The spectral data obtained from the LIBS technique has also been successfully applied for classification of various types of samples by using machine learning algorithms [27], [28], [29]. ANN and PLS-DA are the commonly used supervised learning algorithms. PLS-DA being a binary classification model, its complexity increases in case of multiclassification models [30]. Also, ANN technique has reflected high classification accuracy when compared to other techniques such as PCA, while classifying the aged epoxy samples based on level of ageing as well as type of ageing [31]. Hence, due to factors such as high accuracy, repeatability and faster computation time, the classification capacity of ANN model has improved when compared to other techniques [32]. Therefore, by considering the above advantages of ANN technique, it has been employed in the present study to classify the LIBS spectral data of gamma irradiated SR specimens with respect to level of ageing.

Having known all these, the following methodical experimental studies have been carried out to understand (i) the hydrophobicity recovery characteristics from static contact angle measurement (ii) surface morphological analysis after irradiation from AFM studies (iii) the variation in fractal dimension and lacunarity (iv) thermal stability analysis by thermogravimetric analysis (TGA) (v) variation in LIBS emission spectra and plasma temperature after gamma irradiation and (vi) classification of SR samples based on gamma radiation dose by adopting artificial neural network (ANN) technique to normalized LIBS spectral data.

II. EXPERIMENTAL STUDIES

A. MATERIALS AND METHOD OF SAMPLE PREPARATION

ATH micro particles (average size of 5-10 μm, 99.9% purity, Astrra chemicals, India) and alumina nanoparticles (average

TABLE 1. Composition details of SR specimen.

Specimen name	Base Material (SR) (wt%)	Micro-particle (ATH) (wt%)	Nanoparticle (Alumina) (wt%)
S0	100	0	0
S1	60	40	0
S2	57	40	3

size of 100 nm 99.9% purity, Hongwu Nano-meter, China) are used as filler material to prepare silicone rubber micro-nanocomposites. In order to remove the moisture content, the filler particles were heated in the oven at 150°C (which higher than evaporation temperature) for 24 hours. Furthermore, the weight of the filler particles has been measured before and after drying in the oven. The reduction in the weight of filler particles indicate the removal of moisture from the fillers. The required amount of particles are then mixed with 100 ml of ethanol solution by using shear mixer for 30 minutes. For the proper dispersion of fillers with solvent, the sonication process is done for 30 minutes using an ultra-sonicator with a 9s ON and 9s OFF mode. In the present study, 40% of the overall power rating (750W) has been used for the sonication process. The total energy given for the sonication process is 7.2kJ for 30 minutes. The filler solution is added to silicone rubber (RTV8112, Momentive, USA) and then shear mixed for 30 minutes. The ethanol is removed by keeping the mixture in oven at 100°C. The ethanol free mixture is added with the curing agent (Hardener RTV9858) at the ratio of 10:1 and degassed for 3 minutes for the removal of air bubbles present in the mixture. The final mixture is casted into a square mold and compressed at room temperature for 24 hours with a uniform pressure of 200 kPa. The complete details about the prepared samples are shown in Table 1.

From the recent literature, the impact of gamma ray irradiation at high dosages on polymeric materials has been investigated by several researchers and have indicated that the electrical, mechanical as well as thermal properties are significantly deteriorated by radiation induced degradation reactions [15], [33], [34]. Kaneko et al. have indicated that the exposure of polymeric materials to gamma irradiation at 0.1 kGy/h for 2000 h at high temperatures (200 °C) corresponds to the ageing caused by the normal operation of a nuclear power plant for 85 years at a typical radiation dose rate of 0.34 Gy/h [7]. Thus, with a typical dosage rate of 0.34 Gy/h, the total dosage level of 50 kGy can simulate the impact which is similar to the normal operation of a nuclear power plant for 20 years. Therefore, in order to investigate the influence of low dosage gamma irradiation on the surface properties of the SR insulating material, the test specimens are subjected to radiation dosage of 5 kGy, 10 kGy, 15 kGy and 50 kGy respectively. The diagnostic studies were carried out immediately after the samples were taken out from the gamma ray irradiation chamber.

B. STATIC CONTACT ANGLE AND FTIR ANALYSIS

The contact angle was measured by sessile droplet method. Static contact angle measurement setup with model number of ACAMS10N3, manufactured by Apex Instruments Co. Pvt. Ltd., India, has been used in present study. Deionized (DI) water droplet with the volume of 20 μL is placed on the surface of the specimen and the measurements were carried out. The contact angle was measured at five different locations on the surface of the specimen and the average was taken as final value. To understand the hydrophobicity recovery characteristics, the contact angle was measured with the sample at required time instant. The measurements were carried out until the value reaches saturation. To understand the characteristic variation in functional groups of silicone rubber and composites due irradiation, a Fourier transform infrared spectroscopy analysis was performed in the current study. For FTIR analysis, instrument with model number: A Cary 630 FTIR, manufactured by Santa Clara, USA was adopted.

C. ATOMIC FORCE MICROSCOPY (AFM)

The surface morphology studies of gamma irradiated silicone rubber and its composites were analysed by using Atomic Force Microscopy (A100 AFM, A.P.E Research Srl, Italy). The sample area of 10×10 μm was analysed with a resolution of 256×256 pixels. The 2D and 3D morphology figures are extracted by using Gwyddion software.

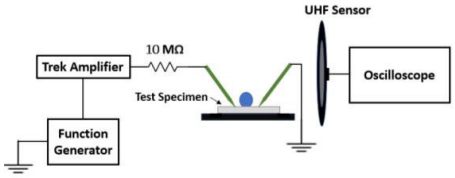

FIGURE 1. Experimental setup for water droplet-initiated discharge studies.

D. WATER DROPLET INITIATED CORONA INCEPTION STUDIES

The experimental setup for measuring water droplet initiated corona inception voltage is shown in Fig 1. It includes a signal generator (Tektronix 3051C), a high voltage amplifier (Trek type 20/20 C), and stainless-steel electrodes with a 45° cut at the tip, as per IEC 60112. The complete procedure for measuring for CIV is explained in the previous study [35].

E. THERMOGRAVIMETRIC ANALYSIS (TGA)

To determine the thermal stability of SR composites after irradiation, thermogravimetric analysis (TGA) has been performed. A TGA equipment Labsys evo, from Setaram instruments, France was used to perform the thermogravimetric analysis on the samples. A 30 mg of each unfilled and composite samples are used, and the temperature range is selected as 30 °C to 650 °C with the heating rate of 20 °C /min at argon ambience.

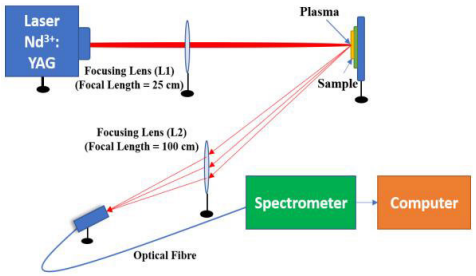

FIGURE 2. Experimental setup for Laser-Induced Breakdown Spectroscopy.

F. LASER-INDUCED BREAKDOWN SPECTROSCOPY

The elemental analysis of the samples is performed by using LIBS technique and the experimental set up is shown in Fig 2. The laser pulse is generated by using a Q-switch driven Nd^{3+}: YAG laser of model number: LAB-150-10-S2K, manufactured by Quanta-Ray LAB series, Spectra Physics, France, with the wavelength of 1064 nm and the pulse duration of 10 ns with 10 Hz repetition rate. A focusing lens (L1), at a focal length of 25 cm from the laser is used to focus the emitted laser on the target. For collecting the emitted radiation from the plasma of the sample an another focusing lens (L2) is used at a focal length of 100 cm from the sample and the emitted radiations were guided to Ocean insight QE Pro spectrometer through an optical fiber with a diameter of 400 μm.

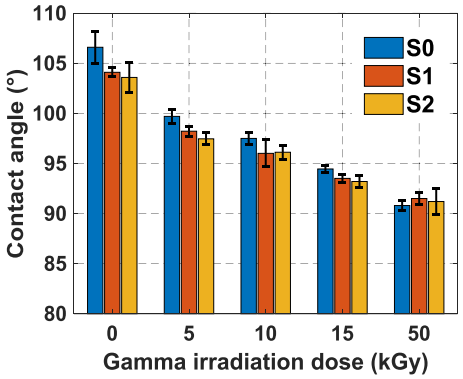

FIGURE 3. Variation in static contact angle with different doses of gamma irradiation.

III. RESULTS AND DISCUSSIONS

A. STATIC CONTACT ANGLE AND HYDROPHOBICITY RECOVERY MEASUREMENT

Fig 3. shows the variation in static contact angle during of the gamma irradiated specimen during recovery period. It is observed that silicone rubber nanocomposites are hydrophobic material, as its contact angle values are more than 90°. The methyl group in the silicone elastomers is the main cause for the hydrophobic nature of the silicone rubber surface [36]. A marginal reduction in contact angle was observed on addition of fillers to silicone rubber, which could be due to the hydrophilic nature of ATH fillers [37].

With increase in gamma radiation dosage, the static contact angle values are noticed to reduce significantly. With the 50 kGy irradiated specimens, the contact angle reduction is high with unfilled silicone rubber compared to the micro nanocomposites. The structural variations that occur due to chain scission and oxidation process due to exposure of gamma rays had deteriorated the surface profile of the silicone rubber sample [38] and this could be a cause for the reduction in contact angle after irradiation.

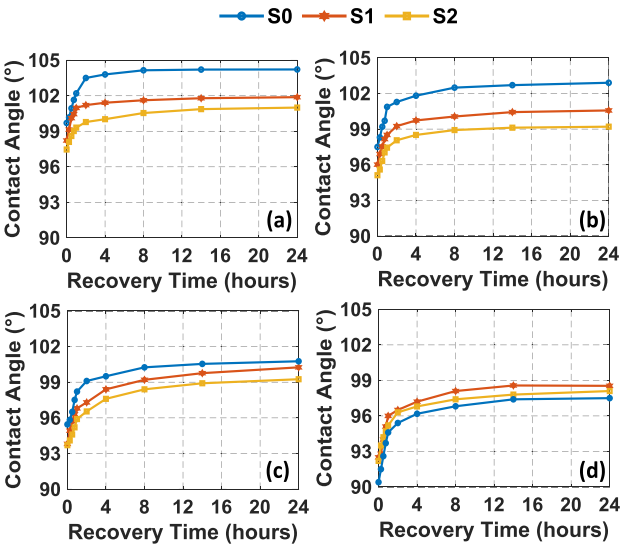

FIGURE 4. Hydrophobicity recovery of SR composites with Gamma Irradiation level of a) 5 kGy, b)10 kGy, c)15 kGy and d)50 kGy.

The variation in hydrophobicity recovery of silicone rubber micro nanocomposites, after the gamma irradiation is shown in Fig 4. The recovery characteristics were determined by measuring the contact angle values of the samples immediately after taken out from the gamma chamber till reaching the steady state contact angle value. It is observed that, the unfilled silicone rubber sample S0 showed the faster hydrophobicity recovery. In silicone rubber, the migration of low molecular weight (LMW) molecules from bulk to surface is the main reason for the recovery for the surface recovery [39]. Due to free migration of LMW molecule, with the unfilled specimen, the fast recovery is achieved. The addition of fillers restricts the migration of LMW molecules and slows down the recovery process. With increase in gamma irradiation dose, the recovery process of contact angle has slowed down (Fig 4). It is because of the reduction in -CH_3 groups with increasing gamma irradiation, which enhances the chain scission process leading to the change in the hydrophobicity of the material and this can be verified from the results of FTIR analysis.

Fig 5. shows the FTIR spectrum of samples S0 and S2 before and after 50 kGy irradiation. The reduction in the absorbance values of methyl functional groups such as Si-CH_3, Si-O-Si and Si-$(CH_3)_2$ at wavenumbers 1257 cm^{-1}, 1012 cm^{-1} and 788 cm^{-1} has been observed, respectively. In the micro-nanocomposite specimens, the presence of

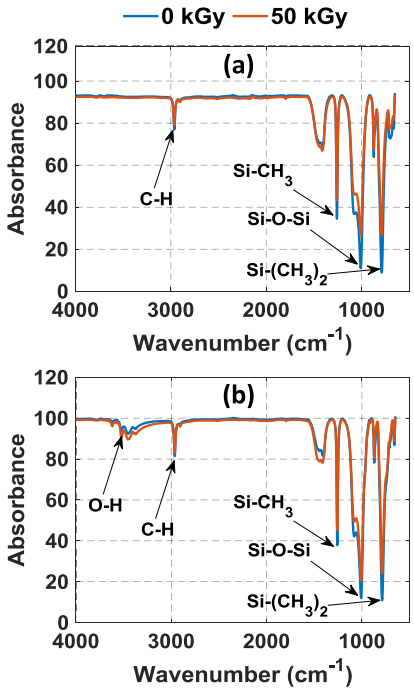

FIGURE 5. FTIR spectrum of sample a) S0 and b) S2 before and after 50 kGy irradiation.

ATH fillers can be observed from the various small peaks (O-H) between the wavenumber 3700 – 3200 cm^{-1} in Fig 5b. The reduction in the absorbance values of peaks has been observed high in unfilled sample (S0) compared to micro-nano nanocomposite sample (S2). The reduction in the FTIR absorbance values of samples after irradiation indicates the reduction in methyl groups of silicone rubber due to the occurrence of surface degradation and chain scission process in the samples [40].

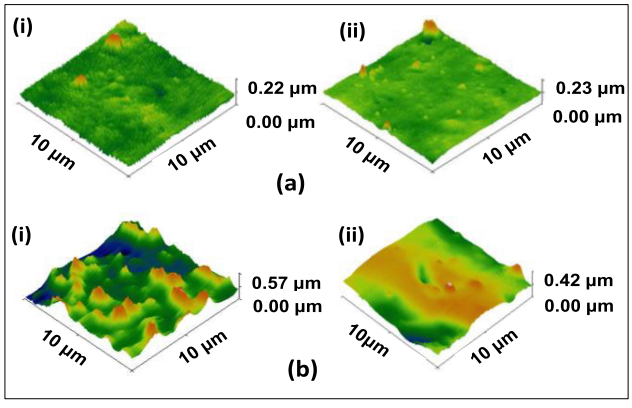

FIGURE 6. 3-D surface plot obtained for samples (i) S0, (ii) S2 (a) before irradiation and (b) after 50 kGy irradiation.

B. ATOMIC FORCE MICROSCOPY

Fig 6. shows a typical 3-D morphology of silicone rubber samples S0 and S2, before and after 50 kGy irradiation. It is observed that, on irradiation, a significant uneven surface is observed with the irradiated specimens. The exposure to radiation has resulted in the chemical and structural changes on the surface of the tests samples leading to the deterioration in their surface profile [38]. The 3D-surface profile of sample S0 is noticed to degrade substantially compared to micro nano composite sample S2 after irradiation (Fig 6b).

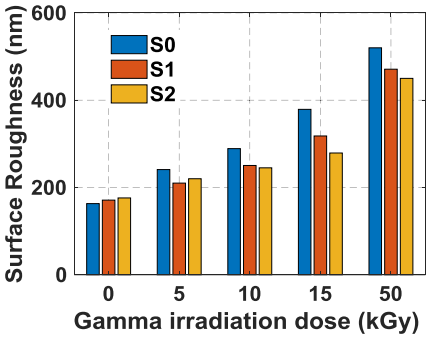

FIGURE 7. Average surface roughness values of samples with different gamma irradiation doses.

The average surface roughness of the gamma irradiated silicone rubber samples measured from the AFM surface profile data is shown in Fig 7. No significant variation is observed with the surface roughness of unaged silicone rubber samples added with different wt% of filler content. After irradiation, increment in surface roughness has been observed in all three samples. The specimen S2 has shown lesser surface roughness of all the test samples after irradiation. The addition of alumina nanoparticles to silicone matrix leads to the formation of strong hydrogen bonding between the alumina nanoparticles and silicone rubber matrix [20], which limits the degradation caused due to gamma irradiation. Comparing the Fig 3 and 7, it is observed that the average surface roughness and static contact angle values with the gamma irradiated specimens shows inverse relationship.

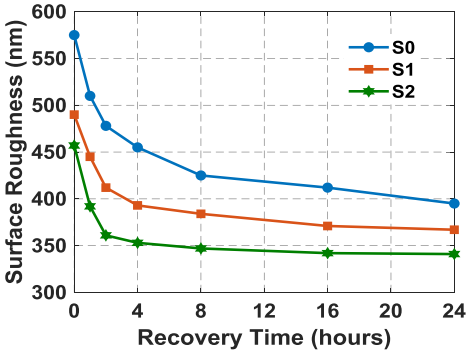

FIGURE 8. Surface roughness recovery plot of samples after 50 kGy gamma irradiation.

To understand the surface recovery characteristics of the gamma irradiated specimens analysed through the measure of surface roughness using AFM studies. The mean surface roughness values of irradiated samples during surface recovery process are shown in Fig 8. The addition of fillers

to silicone rubber matrix restricts the transportation of LMW component from bulk to the surface of silicone rubber and resulted in suppression of rate of recovery in composites compared to pure silicone rubber specimen.

C. FRACTAL DIMENSION AND LACUNARITY

The 3D surface profile data of the test silicone rubber specimens obtained from AFM studies have been used to calculate the fractal dimension. Kolmogorov capacity (or box-counting dimension) measurement is the most popular straightforward, and efficient method for fractal dimension estimation. However, due to the pixel limitations in small box scale, typical box-counting methods based on images may not always be correct. Therefore, fractal dimension measurement using different methods will provide a better analysis. In addition to 3-D box counting method, variogram method and power spectrum method are employed for fractal dimension calculation.

1) 3-D BOX COUNTING METHOD

The 3D box counting technique has been adopted to measure the fractal dimension [41]. A cubic lattice with a specific lattice constant is superimposed on z-expanded surface. The size of cube is selected that all cube contains at least one pixel of the image. The process repeated with the reduced lattice constant by a stepwise factor of 2, until equals to the distance between two adjacent pixels. From the slope of log – log plot between the number of all cubes and inverse of lattice constant the fractal dimension is determined.

2) VARIOGRAM METHOD

In variogram method fractal dimension is measured by calculating the variance of interpixel differences and their relationship to distance. By using a log-log plot of the variance of increments vs increments, it is possible to determine the fractal dimension of the function z(x):

$$Var\,(x) = x^{2H} \tag{1}$$

The variogram method of measuring the fractal dimension has the benefit of being a simple method to use, does not use any complex data adaption. The entire 256 × 256 matrix of the images were scanned to determine the intensity differences in the horizontal and vertical directions of the images. The process was repeated with progressively larger pixel step increments by starting with a pixel step size of 1.

3) POWER SPECTRUM METHOD

The Fourier power spectrum P (ω) of the function can be used to describe the fractal dimension of the function z(x) since it exhibits a power spectrum that decreases with increasing frequency ω and is proportional to:

$$P\,(\omega) = \omega^{-(2H+1)} \tag{2}$$

The co-dimension H and the fractal dimension D can be calculated by performing a linear regression on the log-log plot of the observed power spectrum (PWS) as a function of frequency. The one-dimensional form of the fast Fourier transform (FFT) was used more frequently to save processing time and to make the power spectrum method simpler. In this one-dimensional method, the 256 transect lines that make up the image were subjected to a series of FFT computations. The data created by the recombination of imaginary and real parts of the transform is used to calculate the plane wave spectrum (PWS). To minimize the effect of microstructure and statistical errors, the 256 power spectra from serial sections were averaged. Finally, a log-log plot was created from this average PWS and the slope from the linear regression fit technique was used to estimate the fractal dimension.

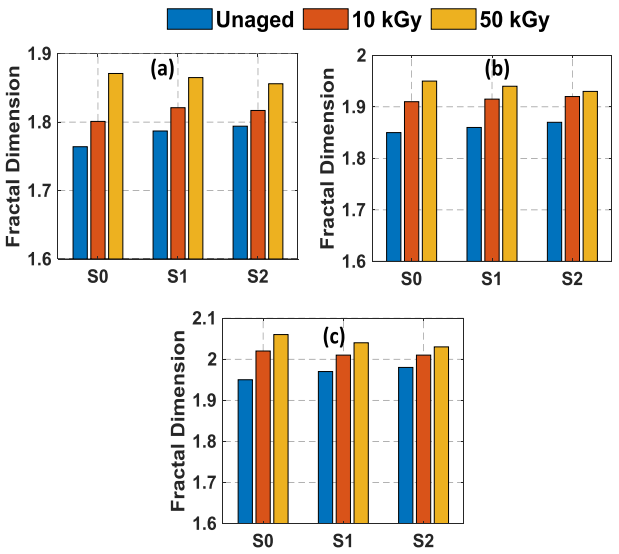

FIGURE 9. Fractal dimension of samples with a) 3D box counting method, b) variogram method and c) power spectrum method.

The variation in fractal dimension by 3D box counting method, variogram and power frequency methods of S0, S1 and S2 with gamma irradiation of 10 kGy and 50 kGy is shown in Fig 9. The fractal dimension determined by using different techniques have followed the same pattern. A significant increase in fractal dimension is observed with gamma irradiated samples compared to unaged samples. Sample S2 with micro and nano fillers exhibited lesser fractal dimension compared other test samples, after irradiation dose of 50 kGy. It is observed that the average surface roughness and the fractal dimension measured using surface profile of specimen using AFM studies showed direct correlation. Lacunarity is used to investigate the inhomogeneity of the material surface by measuring the density of the fractal surface [42]. The variation in lacunarity of unaged, 10 kGy and 50 kGy silicone rubber composites are shown in Fig 10. Significant increase in lacunarity of the test samples after irradiation is an indication for the surface degradation of samples after irradiation. Also, the lacunarity values after 50 kGy irradiation dose have indicated that the surface

degradation is marginally lesser in case of sample S2 when compared to other specimens (Fig 10).

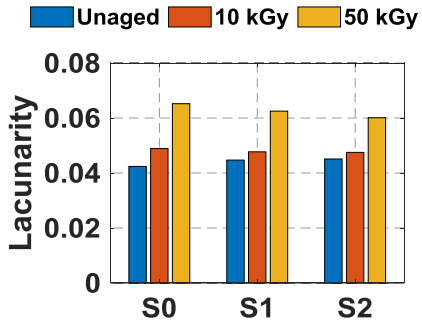

FIGURE 10. Variation in lacunarity of silicone rubber samples.

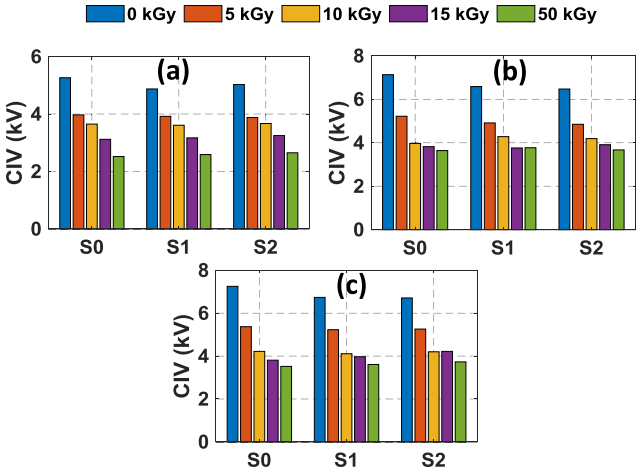

FIGURE 11. Variation in CIV due to different irradiation levels under a) AC, b) positive DC and c) negative DC voltages.

D. WATER DROPLET INITIATED CORONA INCEPTION STUDIES

Fig 11 and 12 shows the variation in CIV of test specimens after irradiation and 24 hours recovery after irradiation. The marginal reduction in CIV has been observed with the addition of fillers. This can be correlated with the reduced hydrophobicity of samples with the addition of fillers. Also, a reduction in CIV is observed with the increased irradiation level. As the surface roughness increases with the gamma irradiation level, the contact angle reduces leading to the increment in the spreading of water droplet on the surface of the specimen. Thus, the water droplet initiated CIV values are significantly reduced after irradiation.

Compared to unfilled sample S0, micro-nano composite sample S2 shows high CIV values after irradiation, indicating that the unfilled sample has damaged more compared to micro-nanocomposite specimen. The rate of change in voltage under AC is more unlike DC, leading to lesser CIV values under AC when compared to DC [43]. Under positive DC, the number of high energy electrons available for initiating the corona phenomena at the tip of the electrodes are

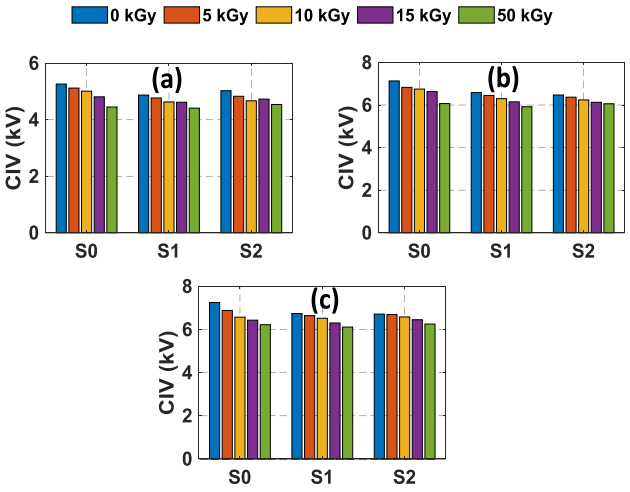

FIGURE 12. Variation in CIV due to different irradiation levels under a) AC, b) positive DC and c) negative DC voltages after 24 hours of recovery.

more than number of such electrons under negative DC [44]. Thus, the CIV values have followed the trend AC< positive DC< negative DC. After 24 hours of recovery, in case of all the test samples, the water droplet CIV has almost reached near to the CIV values before irradiation. With the increase in level of irradiation, the recovery of CIV is noticed to be lesser due to the radiation induced surface degradation of the samples.

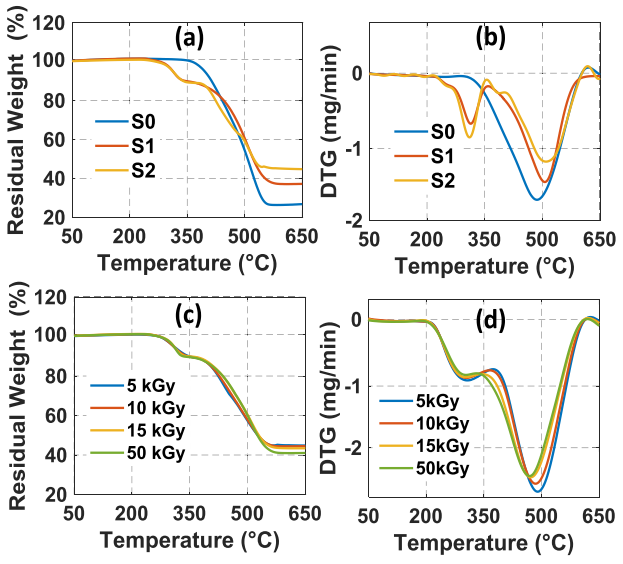

FIGURE 13. Variation in thermogravimetric curves of SR composites (a) TG curves of unaged samples, and (b) their DTG curves, (c) TG curves of sample S2 with different gamma irradiation doses and (d) their DTG curves.

E. THERMOGRAVIMETRIC ANALYSIS (TGA)

Fig 13 shows the TG and DTG curves of the virgin and gamma-irritated samples. The base silicone rubber sample S0 has experienced thermal decomposition after the temperature of about 350 °C, which resulted in a considerable weight loss

in the TG curve. In case of specimens S1 and S2, a small weight loss due to thermal decomposition phenomenon has been noticed at around 200 °C and then followed by a significant weight loss in the specimens above 350 °C. Nazir et al. have observed the similar results in the ATH filled SR composites with initial thermal decomposition in the range of 220 °C to 350 °C. It was attributed to the release of water from the micro-ATH particles which has resulted in the early weight drop of TG curves in samples S1 and S2 [45]. From DTG curves shown in Fig 13b, the maximum thermal degradation temperature (T_{max}) of sample S0 is observed to be 485 °C, and for samples S1 and S2, the T_{max} values are 510 °C and 515 °C respectively. Also, the final residual weight of SR composites (S1 and S2) at 650 °C is significantly higher when compared to base sample S0. This reflects the increased thermal stability of the composites upon the addition of fillers. The variation in the TG and DTG curves of sample S2 with respect to gamma irradiation dosage are given in Fig 13c and Fig 13d respectively. The maximum decomposition temperature of the gamma irradiated S2 specimens is noticed to reduce with respect to increase in the dosage of gamma irradiation. The radiation induced degradation reactions such as chain scission and oxidation tend to reduce the thermal stability of the samples, leading the samples to thermally decompose at relatively lower temperatures than that of the unaged samples [38].

Further, the TG curves are used to determine the thermal activation energy (E_a) of the unaged and gamma irradiated SR composite specimens. Thermal activation energy is the minimum energy required for the samples to the initiate a thermal degradation reaction [46]. Depending on either the rate of conversion or the rate of heating, different thermogravimetric approaches have been used to determine the thermal kinetic parameters. Utilizing the method recommended by Horowitz and Metzger [47], the activation energy of thermal degradation can be determined from the TG curves using (3).

$$ln\left\{ln\left[\frac{(W_o - W_f)}{(W - W_f)}\right]\right\} = \left(\frac{E_a}{RT_s^2}\right)\theta \tag{3}$$

By considering $ln\left\{ln\left[\frac{(W_o - W_f)}{(W - W_f)}\right]\right\} = \mathrm{K}$, (3) becomes

$$K = \left(\frac{E_a}{RT_s^2}\right)\theta \tag{4}$$

W_0 and W_f are the starting and ending stage weights respectively, and R is the universal gas constant. Where W represents the remaining weight of samples at a particular temperature. The difference in temperature between T and T_s is mentioned as θ. T_s is the temperature at which the following equation holds true:

$$\left[\frac{(W - W_f)}{(W_o - W_f)}\right] = \left(\frac{1}{e}\right) = 0.3679 \tag{5}$$

According to the above equation, a plot of K versus θ leads to a straight-line connection which is shown in Fig 14.

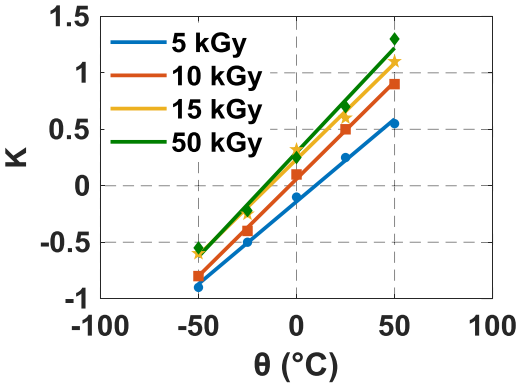

FIGURE 14. K versus θ plot of sample S2 with different irradiation levels.

Therefore, it is possible to determine the activation energy of thermal decomposition, by calculating the slope of the line. The parameters T_s and E_a of virgin and irradiated test samples computed using equations (4) and (5) are tabulated in Table 2. The thermal activation energy and the final residual weight (at 650 °C) have reflected a decreasing trend with increase in gamma irradiation dosage. This indicates that the gamma irradiation is causing a significant impact on the thermal stability of the test samples. Of these samples, sample S2 has exhibited higher activation energy and lesser thermal degradation compared to other samples before and after irradiation.

F. LASER-INDUCED BREAKDOWN SPECTROSCOPY

LIBS analysis has been adopted to understand the impact of gamma irradiation on the surface of silicone rubber and composites. From the NIST database, different elements present in the material have been detected from the LIBS spectral peaks. Fig 15 shows the LIBS spectra of the samples before aging and after gamma irradiation. From the spectral data the peak elements corresponding to Si (I), Si (II), Ca (I), N (I), N (II), C (I), C (II), O (I), and H (I) are observed. The emission spectra of unaged samples are shown in Fig 15(a). In composite samples, high intensity of aluminium peaks demonstrates the addition of ATH and alumina fillers with SR material.

The spectra of sample S2 after different level of gamma radiation are shown in Fig 15 (b). A slight reduction in the magnitude of spectral peak intensity was observed after the gamma exposure in the virgin and composite samples. The samples were allowed to recover, and the LIBS analysis was performed at different period of time. The recovery phase of sample S2 after 50 kGy irradiation is shown in Fig 15 (c). A minor increase in magnitude of peak intensity after certain time periods indicate the recovery of the nanocomposites and, the peak intensity magnitude of samples after 24 h recovery time is found to be almost like the unaged samples. The plasma temperature of the silicone rubber samples by using the LIBS data were calculated by using Boltzmann–Saha

TABLE 2. Thermal parameters for the samples S0, S1 and S2 before and after gamma irradiation.

Samples	S0			S1			S2		
Irradiation level	T_s (°C)	E_a (J/mol)	Residual weight at 650 °C (%)	T_s (°C)	E_a (J/mol)	Residual weight at 650 °C (%)	T_s (°C)	E_a (J/mol)	Residual weight at 650 °C (%)
0 kGy	482.023	918.144	26.73	489.332	946.289	37.17	492.512	956.287	44.77
5 kGy	475.097	868.205	24.50	481.736	893.003	36.82	485.909	908.541	44.72
10 kGy	468.134	824.581	23.72	473.276	843.278	35.73	490.381	856.732	44.50
15 kGy	467.113	771.162	22.93	468.146	774.952	35.52	473.781	812.789	43.42
50 kGy	453.231	682.935	22.61	463.469	714.866	34.20	470.342	736.573	41.02

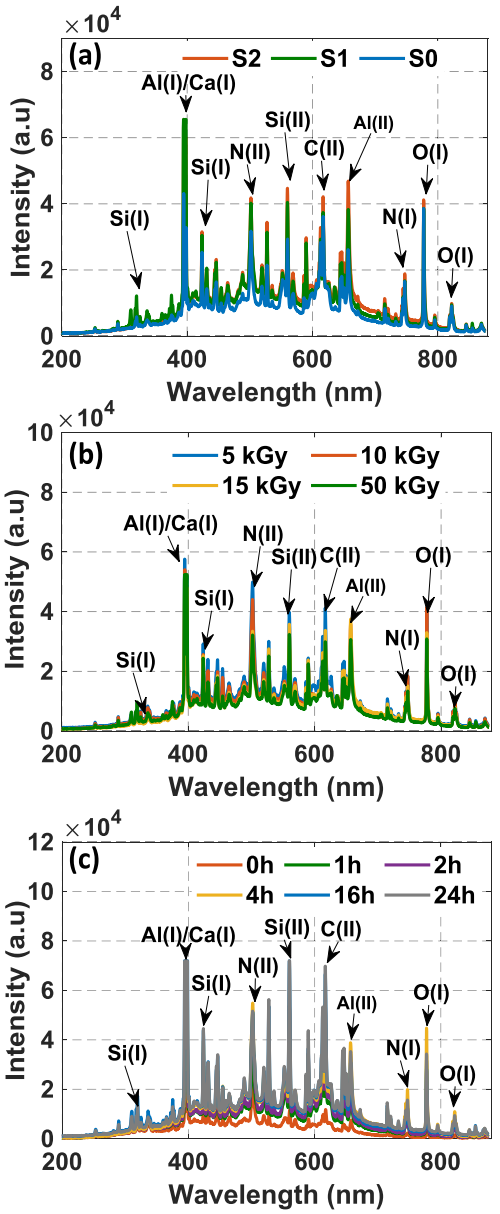

FIGURE 15. Emission spectra of SR samples(a) before irradiation, (b) after irradiation of sample S2 (c) recovery of sample S2 after 50 kGy irradiation.

equation

$$T_e = 1.44 \frac{E_2 - E_1}{ln\left[\frac{l_1 \lambda_1 A_2 g_2}{l_2 \lambda_2 A_1 g_1}\right]} \tag{6}$$

TABLE 3. Complete details of spectral line used for calculating the plasma temperature.

Atom/ion	Wavelength	Intensity peak	Excited energy level
Si (I)	288.1	1.5×10^4	40991.88
Si (II)	594.85	4.3×10^4	57798.08

where E_1 and E_2 are refers to the energy levels excited at peaks 1 and 2, l_1 and l_2 are refers to the atomic species intensities at the wavelength of λ_1 and λ_2, respectively, transition probabilities of states are referred as A_1 and A_2, the statistical weights are referred as g_1 and g_2, and the plasma electron temperature is referred as T_e. For the calculation of plasma temperature, the elemental peaks of Si (I) and Si (II) at the wavelength of 288.1 and 594.85 has been considered, respectively. Table 3 shows the complete details of spectral line used for calculating the plasma temperature.

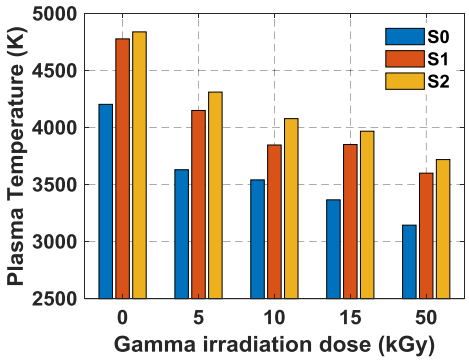

FIGURE 16. Plasma temperature values of SR samples before and after irradiation.

Fig 16 shows the calculated plasma temperature of unaged and gamma exposed silicone rubber samples. The composite samples have greater plasma temperature values when compared to sample S0. The plasma temperature is noticed to decrease with the increase gamma irradiation dose. By utilizing LIBS spectra characterization, Wang et al. have established the examination of surface hardness of an aged HTV silicone rubber insulator. They have also observed a linear relationship between the surface hardness of the silicone rubber sample and the average plasma temperature. The strong interfacial adhesion between the added fillers and silicone rubber matrix subsequently increases the plasma

temperature of the material [48]. Hence, the higher plasma temperature in composite specimens (S1 and S2) indicate the superior surface hardness, when compared to virgin sample. The micro-nano composite sample S2 has the highest electron density due to the good dispersion of nano and micro particles along with the siloxane bond. Due to the reduction in -CH_3 content with increasing irradiation induced chain scission process, the surface hardness of the material had reduced. This led to the reduction in the plasma temperature of the test specimens with increment in irradiation dosage.

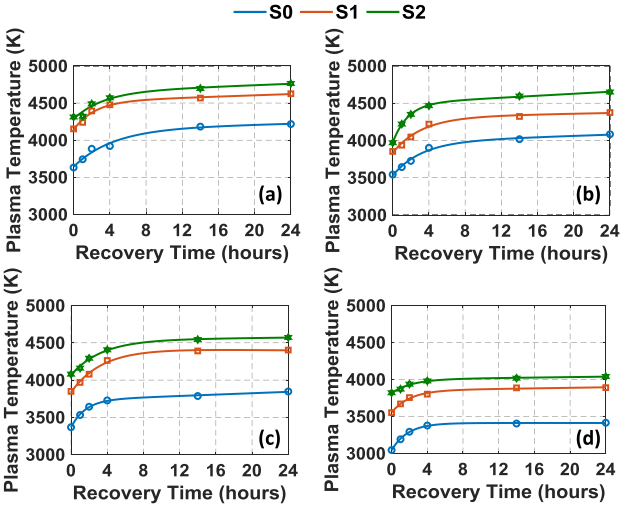

FIGURE 17. Plasma temperature characteristics of SR composites with gamma irradiation level of a) 5 kGy, b)10 kGy, c)15 kGy and d) 50 kGy.

Further, the silicone rubber samples are allowed to recover and at different recovery times the plasma temperature has been calculated. Fig 17 shows the recovery in plasma temperature after the exposure of gamma ray irradiation. The migration level of LMW components is the main factor which influences the surface recovery rate. A marginal reduction in recovery rate has been observed with the increased irradiation dose. This can be attributed to the radiation induced degradation reactions which have affected the migration of LMW components in the SR material. The plasma electron density was estimated using the following equation:

$$n_e = 6.6\times10^{21}\frac{I_a A_i g_i}{I_i A_a g_a}\exp\left(-\frac{E^{ion}+E_i-E_a}{T}\right) \quad (7)$$

where the ionic and atomic species energies of the excited energy levels are referred as E_i and E_a, statistical weights are referred as g_i and g_a, transition probabilities of states are referred as A_i and A_a, the wavelengths are λ_1, λ_2 and the intensities of ionic and atomic species are referred as I_i and I_a respectively, ionization energy is defined as E^{ion} and plasma electron density is defined as n_e under the local thermodynamic equilibrium.

Fig 18 shows the electron density values of samples S0, S1 and S2. The reduction in election densities is found with the higher gamma doses. The molecular changes due to the

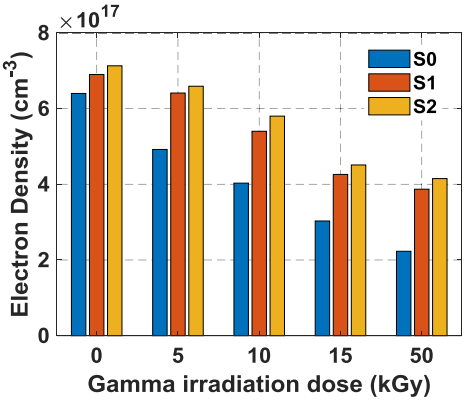

FIGURE 18. Plasma electron density of SR samples before and after irradiation.

chain scission and reduction in methyl groups from silicone rubber samples with the exposure of irradiation, reduced the plasma electron density. The electron density values of the test specimens during recovery period have followed same trend as that of the plasma temperature values during recovery (Fig 19).

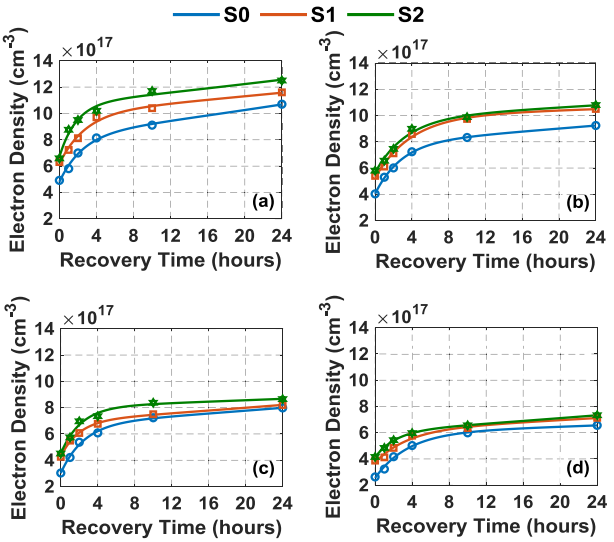

FIGURE 19. Recovery of electron density of SR composites after gamma irradiation level of a) 5 kGy, b)10 kGy, c)15 kGy and d)50 kGy.

The crater formed by the laser ablation after 100 pulses with the time interval of 0.1s on each sample has been measured using a non-contact surface profilometer. The depth of crater formed on the samples with various irradiation doses is shown in Fig 20. Sample S0 has a deeper crater than other samples, which indicates that characteristic variation in material properties is observed high with the specimen. This clearly indicates that the filler added specimen shows high radiation resistant.

G. ADOPTING ANN ANALYSIS TO LIBS

The normalized LIBS spectral data has been used to classify the virgin silicone rubber and its composites based on the

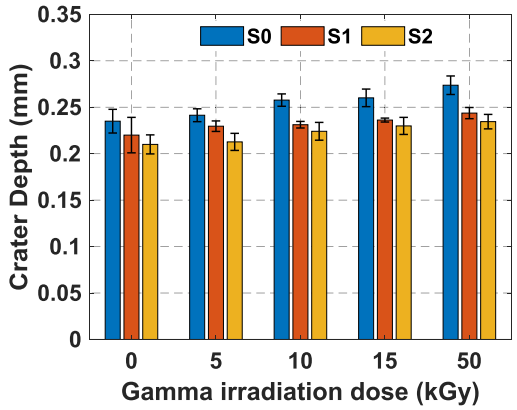

FIGURE 20. Crater depth value of samples before and after irradiation.

TABLE 4. Different combinations of the input dataset distribution.

Combination	Selected data (%)		
	Training	Validating	Testing
C1	80	10	10
C2	70	15	15
C3	60	20	20

gamma irradiation level, by adopting ANN algorithm. The samples are categorized using an ANN model with two-layer forwarding architecture with a hidden layer and an output layer (Fig 21).

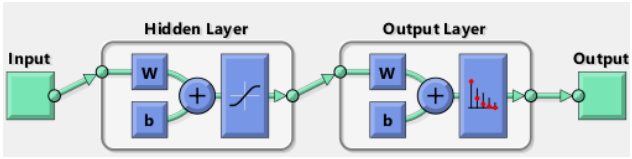

FIGURE 21. The architecture of artificial neural network.

A matrix with the dimension of 200 × 2048 formed by the normalized LIBS intensity data of gamma irradiated sample with dosage levels of 5 kGy, 10 kGy, 15 kGy and 50 kGy has been chosen as the input data set. Out of 200 observations each 50 observations belong to one level of radiation, respectively. The input dataset is divided in the three sub-divisions such as training, validation and testing data sets. The number of neurons in the hidden layer should be selected properly because it can affect the performance of neural network [31]. Also, the proper distribution of input data to the training, validating and testing data sets may lead to achieve better classification. Hence, in this study, the number of neurons in the hidden layer is varied from 2 to 30 with the three combinations of input data distribution as shown in Table. 4. The optimized combination of input data distribution and number of hidden neurons has been selected based on the convergence of number of epochs (the number of iterations) used in classification.

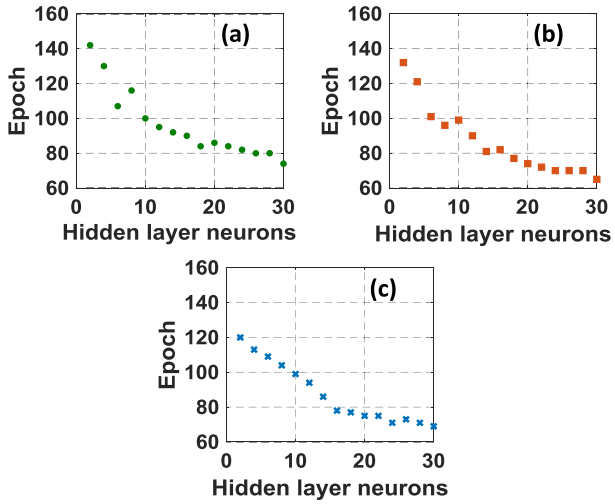

FIGURE 22. Variation in Epoch vs no of hidden neurons with various combinations a) C1, b) C2, and c) C3 of the input dataset distribution.

FIGURE 23. Confusion matrices for the classification of sample S2 with respect to level of gamma irradiation doses.

Fig 22. represents the variation in number of epochs with respect to number of neurons in the hidden layer, for different combinations. The number of epochs required for the convergence tends to reduce with the increase in the number of neurons in the hidden layer. The number of epochs almost converges with the number of neurons of 24, 20 and 18 in hidden layers with the combinations C1, C2 and C3 respectively. Among that combination C2 converges with least number of epochs with 20 neurons in hidden layer and almost equals the number of epochs with combination C3. Hence, the combination C2 with the distribution of 75%

training set, 15% validation set and 15% testing data of the input data set with 20 neurons in the hidden layer has been obtained as the optimum in the present study for all the three test specimens.

The confusion matrix is developed by using MATLAB software toolbox. Fig 23 depicts the confusion matrix for sample S2 with various gamma dosages. In the confusion matrix, the green colored boxes represent the correctly estimated data while the red colored boxes represent the incorrectly classified data. The silicone rubber micro-nano composite sample S2 is classified accurately with 100% accuracy with respect to various levels of gamma doses. Similarly, the other test specimens are also successfully classified with 100% classification accuracy by using the optimized ANN model. The result of the study clearly indicates that LIBS spectra can be used as a condition monitoring tool enabling one to understand level of irradiation exposed by the specimen. Admittedly further work needs to be carried out to ascertain the acquired results further and to generalize the procedure with different materials, to use LIBS as enabler for understanding the level of irradiation.

IV. CONCLUSION

The important conclusions based on the study are follows:

- A significant reduction in static contact angle values has been observed with silicone rubber and with silicone rubber micro nanocomposites, on gamma irradiation of the specimen. A reduction in rate of recovery was also observed with increasing irradiation of the specimen and is predominant with micro nanocomposites.
- An inverse correlation between the hydrophobicity and mean surface roughness of the material has been noticed. Fractal dimension and lacunarity values follow the same trend as the average surface roughness measured with the specimen.
- FTIR analysis indicates that the micro nano composite sample S2 shows less degradation compared to virgin sample.
- TGA studies clearly indicated that the filler added samples have exhibited higher thermal activation energy and lesser thermal degradation compared to unfilled sample, even on irradiation.
- The plasma temperature and the electron density calculated from LIBS spectra were noticed to reduce marginally, on irradiation. The crater depth formed due to laser ablation was noticed to be lower with silicone rubber micro nanocomposites when compared to base SR.
- The ANN method was able to classify the SR samples effectively according to the level of gamma irradiation. The classification accuracy of 100% was achieved by choosing the appropriate number of hidden layer neurons and by selecting proper input dataset distribution.

Overall, it can be concluded that the silicone rubber micro-nanocomposite sample S2 filled with micro-ATH and nano Alumina fillers has been noticed to be radiation resistive over other test specimens.

REFERENCES

[1] Y. Song, J. Yu, D. Dai, L. Song, and N. Jiang, "Effect of silica particles modified by in-situ and ex-situ methods on the reinforcement of silicone rubber," *Mater. Des.*, vol. 64, pp. 687–693, Dec. 2014, doi: 10.1016/j.matdes.2014.08.051.

[2] Y. Xue, X. Li, H. Wang, F. Zhao, D. Zhang, and Y. Chen, "Improvement in thermal conductivity of through-plane aligned boron nitride/silicone rubber composites," *Mater. Des.*, vol. 165, Mar. 2019, Art. no. 107580, doi: 10.1016/j.matdes.2018.107580.

[3] L. H. Meyer, E. A. Cherney, and S. H. Jayaram, "The role of inorganic fillers in silicone rubber for outdoor insulation alumina tri-hydrate or silica," *IEEE Elect. Insul. Mag.*, vol. 20, no. 4, pp. 13–21, Jul. 2004, doi: 10.1109/MEI.2004.1318835.

[4] B. Venkatesulu and M. Thomas, "Erosion resistance of alumina-filled silicone rubber nanocomposites," *IEEE Trans. Dielectr. Electr. Insul.*, vol. 17, no. 2, pp. 615–624, Apr. 2010, doi: 10.1109/TDEI.2010.5448119.

[5] Y. Liu, D. Zhang, H. Xu, S. M. Ale-emran, and B. X. Du, "Characteristic analysis of surface damage and bulk micro-cracks of SiR/SiO_2 nanocomposites caused by surface arc discharges," *IEEE Trans. Dielectr. Electr. Insul.*, vol. 23, no. 4, pp. 2102–2109, Aug. 2016, doi: 10.1109/TDEI.2016.7556484.

[6] M. T. Nazir, B. T. Phung, S. Yu, and S. Li, "Resistance against AC corona discharge of micro-ATH/nano-Al_2O_3 co-filled silicone rubber composites," *IEEE Trans. Dielectr. Electr. Insul.*, vol. 25, no. 2, pp. 657–667, Apr. 2018, doi: 10.1109/TDEI.2018.006914.

[7] T. Kaneko, S. Ito, T. Minakawa, N. Hirai, and Y. Ohki, "Degradation mechanisms of silicone rubber under different aging conditions," *Polym. Degradation Stability*, vol. 168, Oct. 2019, Art. no. 108936, doi: 10.1016/j.polymdegradstab.2019.108936.

[8] A. M. Abd El-Hameed, "Radiation effects on composite materials used in space systems: A review," *NRIAG J. Astron. Geophys.*, vol. 11, no. 1, pp. 313–324, Dec. 2022, doi: 10.1080/20909977.2022.2079902.

[9] C. V. More, Z. Alsayed, M. S. Badawi, A. A. Thabet, and P. P. Pawar, "Polymeric composite materials for radiation shielding: A review," *Environ. Chem. Lett.*, vol. 19, no. 3, pp. 2057–2090, 2021, doi: 10.1007/s10311-021-01189-9.

[10] H. Alavian, A. Samie, and H. Tavakoli-Anbaran, "Experimental and Monte Carlo investigations of gamma ray transmission and buildup factors for inorganic nanoparticle/epoxy composites," *Radiat. Phys. Chem.*, vol. 174, Sep. 2020, Art. no. 108960, doi: 10.1016/j.radphyschem.2020.108960.

[11] S. T. Lai, "A critical overview on spacecraft charging mitigation methods," *IEEE Trans. Plasma Sci.*, vol. 31, no. 6, pp. 1118–1124, Dec. 2003, doi: 10.1109/TPS.2003.820969.

[12] A. Roggero, E. Dantras, T. Paulmier, C. Tonon, N. Balcon, V. Rejsek-Riba, S. Dagras, and D. Payan, "Electrical behaviour of a silicone elastomer under simulated space environment," *J. Phys. D, Appl. Phys.*, vol. 48, no. 13, Apr. 2015, Art. no. 135302, doi: 10.1088/0022-3727/48/13/135302.

[13] B. Du, Y. Gao, and Y. Liu, "Effects of gamma-ray irradiation on tracking failure of polymer insulating materials," in *Nuclear Power Operation, Safety and Environment*. London, U.K.: IntechOpen, 2011.

[14] B. Thangabalan, R. Sarathi, N. Harid, and H. Griffiths, "Analysis of space charge and charge trap characteristics of gamma irradiated silicone rubber nanocomposites," *IET Nanodielectrics*, vol. 3, no. 2, pp. 44–52, Jun. 2020, doi: 10.1049/iet-nde.2019.0041.

[15] D. Min, C. Yan, Y. Huang, S. Li, and Y. Ohki, "Dielectric and carrier transport properties of silicone rubber degraded by gamma irradiation," *Polymers*, vol. 9, no. 10, p. 533, 2017, doi: 10.3390/polym9100533.

[16] M. Fu, G. Chen, L. A. Dissado, J. C. Fothergill, and C. Zou, "The effect of gamma irradiation on space charge behaviour and dielectric spectroscopy of low-density polyethylene," in *Proc. IEEE Int. Conf. Solid Dielectrics*, Jul. 2007, pp. 442–445, doi: 10.1109/ICSD.2007.4290846.

[17] Y. L. Hsieh, G. Barrall, and S. Xu, "Effects of oxidation on mechanical and physical properties of ultra-high-modulus and ultra-high-molecular-weight polyethylene fibres," *Polymer*, vol. 33, no. 3, pp. 536–545, 1992, doi: 10.1016/0032-3861(92)90730-K.

[18] T. Tokoro and R. Hackam, "Loss and recovery of hydrophobicity and surface energy of HTV silicone rubber," *IEEE Trans. Dielectr. Electr. Insul.*, vol. 8, no. 6, pp. 1088–1097, Dec. 2001, doi: 10.1109/94.971469.

[19] A. Tóth, I. Bertóti, M. Blazsó, G. Bánhegyi, A. Bognar, and P. Szaplonczay, "Oxidative damage and recovery of silicone rubber surfaces. I. X-ray photoelectron spectroscopic study," *J. Appl. Polym. Sci.*, vol. 52, no. 9, pp. 1293–1307, May 1994, doi: 10.1002/app.1994.070520914.

[20] Neelmani, B. Thangabalan, N. J. Vasa, B. Srinivasan, H. Suematsu, and R. Sarathi, "Investigation on surface condition of the corona-aged silicone rubber nanocomposite adopting wavelet and LIBS technique," *IEEE Trans. Plasma Sci.*, vol. 49, no. 8, pp. 2294–2304, Aug. 2021, doi: 10.1109/TPS.2021.3094124.

[21] W. Zahn and A. Zösch, "The dependence of fractal dimension on measuring conditions of scanning probe microscopy," *Fresenius' J. Anal. Chem.*, vol. 365, nos. 1–3, pp. 168–172, Sep. 1999, doi: 10.1007/s002160051466.

[22] J. Brewer and L. D. Girolamo, "Limitations of fractal dimension estimation algorithms with implications for cloud studies," *Atmos. Res.*, vol. 82, nos. 1–2, pp. 433–454, Nov. 2006, doi: 10.1016/j.atmosres.2005.12.012.

[23] C. Douketis, Z. Wang, T. L. Haslett, and M. Moskovits, "Fractal character of cold-deposited silver films determined by low-temperature scanning tunneling microscopy," *Phys. Rev. B, Condens. Matter*, vol. 51, no. 16, pp. 11022–11031, Apr. 1995, doi: 10.1103/PhysRevB.51.11022.

[24] Q. Huang, J. R. Lorch, and R. C. Dubes, "Can the fractal dimension of images be measured?" *Pattern Recognit.*, vol. 27, no. 3, pp. 339–349, 1994, doi: 10.1016/0031-3203(94)90112-0.

[25] H. R. Griem, *Principles of Plasma Spectroscopy*. Dordrecht, The Netherlands: Springer, 1997.

[26] C. Aragón and J. A. Aguilera, "Characterization of laser induced plasmas by optical emission spectroscopy: A review of experiments and methods," *Spectrochim. Acta B, At. Spectrosc.*, vol. 63, no. 9, pp. 893–916, Sep. 2008, doi: 10.1016/j.sab.2008.05.010.

[27] P. R. Villas-Boas, R. A. Romano, M. A. de Menezes Franco, E. C. Ferreira, E. J. Ferreira, S. Crestana, and D. M. B. P. Milori, "Laser-induced breakdown spectroscopy to determine soil texture: A fast analytical technique," *Geoderma*, vol. 263, pp. 195–202, Feb. 2016, doi: 10.1016/j.geoderma.2015.09.018.

[28] G. Yang, S. Qiao, P. Chen, Y. Ding, and D. Tian, "Rock and soil classification using PLS-DA and SVM combined with a laser-induced breakdown spectroscopy library," *Plasma Sci. Technol.*, vol. 17, no. 8, pp. 656–663, Aug. 2015, doi: 10.1088/1009-0630/17/8/08.

[29] B. Campanella, E. Grifoni, S. Legnaioli, G. Lorenzetti, S. Pagnotta, F. Sorrentino, and V. Palleschi, "Classification of wrought aluminum alloys by artificial neural networks evaluation of laser induced breakdown spectroscopy spectra from aluminum scrap samples," *Spectrochim. Acta B, At. Spectrosc.*, vol. 134, pp. 52–57, Aug. 2017, doi: 10.1016/j.sab.2017.06.003.

[30] N. C. Dingari, I. Barman, A. K. Myakalwar, S. P. Tewari, and M. K. Gundawar, "Incorporation of support vector machines in the LIBS toolbox for sensitive and robust classification amidst unexpected sample and system variability," *Anal. Chem.*, vol. 84, no. 6, pp. 2686–2694, Mar. 2012, doi: 10.1021/ac202755e.

[31] M. S. Babu, T. Imai, and R. Sarathi, "Classification of aged epoxy micro–nanocomposites through PCA- and ANN-adopted LIBS analysis," *IEEE Trans. Plasma Sci.*, vol. 49, no. 3, pp. 1088–1096, Mar. 2021, doi: 10.1109/TPS.2021.3061410.

[32] J. Serrano, J. Moros, C. Sánchez, J. Macías, and J. J. Laserna, "Advanced recognition of explosives in traces on polymer surfaces using LIBS and supervised learning classifiers," *Analytica Chim. Acta*, vol. 806, pp. 107–116, Jan. 2014, doi: 10.1016/j.aca.2013.11.035.

[33] A. Shimada, M. Sugimoto, H. Kudoh, K. Tamura, and T. Seguchi, "Degradation mechanisms of silicone rubber (SiR) by accelerated ageing for cables of nuclear power plant," *IEEE Trans. Dielectr. Electr. Insul.*, vol. 21, no. 1, pp. 16–23, Feb. 2014, doi: 10.1109/TDEI.2013.004177.

[34] Z. X. Wu, J. W. Li, C. J. Huang, R. J. Huang, and L. F. Li, "Effect of gamma irradiation on the mechanical behavior, thermal properties and structure of epoxy/glass-fiber composite," *J. Nucl. Mater.*, vol. 441, nos. 1–3, pp. 67–72, Oct. 2013, doi: 10.1016/j.jnucmat.2013.05.041.

[35] J. M. Dhivakar, R. Sarathi, and S. Kornhuber, "Investigation on electrical, thermal, and mechanical properties of silicone rubber ATH nanocomposites," *IEEE Access*, vol. 10, pp. 94040–94050, 2022, doi: 10.1109/ACCESS.2022.3204028.

[36] M. T. Nazir, B. T. Phung, and M. Hoffman, "Performance of silicone rubber composites with SiO_2 micro/nano-filler under AC corona discharge," *IEEE Trans. Dielectr. Electr. Insul.*, vol. 23, no. 5, pp. 2804–2815, Oct. 2016, doi: 10.1109/TDEI.2016.7736840.

[37] G.-H. Liu, B.-H. Zhou, Y.-F. Li, T.-G. Qi, and X.-B. Li, "Surface properties of superfine alumina trihydrate after surface modification with stearic acid," *Int. J. Minerals, Metall., Mater.*, vol. 22, no. 5, pp. 537–542, May 2015, doi: 10.1007/s12613-015-1104-0.

[38] A. S. Palsule, S. J. Clarson, and C. W. Widenhouse, "Gamma irradiation of silicones," *J. Inorganic Organometallic Polym. Mater.*, vol. 18, no. 2, pp. 207–221, Jun. 2008, doi: 10.1007/s10904-008-9205-0.

[39] M. T. Nazir, B. T. Phung, and M. Hoffman, "Performance of silicone rubber composites with SiO_2 micro/nano-filler under AC corona discharge," *IEEE Trans. Dielectr. Electr. Insul.*, vol. 23, no. 5, pp. 2804–2815, Oct. 2016, doi: 10.1109/TDEI.2016.7736840.

[40] L. X. Zhang, S. Y. He, Z. Xu, and Q. Wei, "Damage effects and mechanisms of proton irradiation on methyl silicone rubber," *Mater. Chem. Phys.*, vol. 83, nos. 2–3, pp. 255–259, Feb. 2004, doi: 10.1016/j.matchemphys.2003.09.043.

[41] Y. Gao, X. Liang, W. Bao, S. Li, C. Wu, Y. Liu, and Y. Cai, "Effects of liquids immersion and drying on the surface properties of HTV silicone rubber: Characterisation by contact angle and surface physical morphology," *High Voltage*, vol. 4, no. 1, pp. 49–58, Mar. 2019, doi: 10.1049/hve.2018.5071.

[42] B. X. Du, G. Wei, Y. Wu, and M. Ouyang, "Wavelet-based and fractal theory on partial discharge classification," in *Proc. Int. Symp. Electr. Insulating Mater. (ISEIM)*, Jun. 2005, pp. 463–466, doi: 10.1109/iseim.2005.193589.

[43] M. H. Nazemi and V. Hinrichsen, "Experimental investigations on water droplet oscillation and partial discharge inception voltage on polymeric insulating surfaces under the influence of AC electric field stress," *IEEE Trans. Dielectr. Electr. Insul.*, vol. 20, no. 2, pp. 443–453, Apr. 2013, doi: 10.1109/TDEI.2013.6508746.

[44] J.-R. Riba, A. Morosini, and F. Capelli, "Comparative study of AC and positive and negative DC visual corona for sphere-plane gaps in atmospheric air," *Energies*, vol. 11, no. 10, p. 2671, Oct. 2018, doi: 10.3390/en11102671.

[45] M. T. Nazir, B. T. Phung, S. Yu, and S. Li, "Effects of thermal properties on tracking and erosion resistance of micro-ATH/AlN/BN filled silicone rubber composites," *IEEE Trans. Dielectr. Electr. Insul.*, vol. 25, no. 6, pp. 2076–2085, Dec. 2018, doi: 10.1109/TDEI.2018.007125.

[46] S. A. Nouh and M. M. Abutalib, "Effect of gamma irradiation on the structural, thermal and optical properties of makrofol BL 2–4," *Radiat. Effects Defects Solids*, vol. 169, no. 10, pp. 817–827, Oct. 2014, doi: 10.1080/10420150.2014.956320.

[47] H. H. Horowitz and G. Metzger, "A new analysis of thermogravimetric traces," *Anal. Chem.*, vol. 35, no. 10, pp. 1464–1468, Sep. 1963, doi: 10.1021/ac60203a013.

[48] X. Wang, X. Hong, P. Chen, C. Zhao, Z. Jia, L. Wang, and L. Zou, "Surface hardness analysis of aged composite insulators via laser-induced plasma spectra characterization," *IEEE Trans. Plasma Sci.*, vol. 47, no. 1, pp. 387–394, Jan. 2019, doi: 10.1109/TPS.2018.2870302.

J. MANOJ DHIVAKAR received the M.Tech. degree from NIT Calicut, Calicut, India, in 2021. He is currently pursuing the Ph.D. degree with the High Voltage Laboratory, IIT Madras, Chennai, India.

His primary research interests include preparation and characterization of suitable micro-nanocomposite insulating materials for power systems.

MYNENI SUKESH BABU received the Ph.D. degree in high voltage engineering from the IIT Madras, Chennai, India, in 2022.

He is currently working as a Postdoctoral Equivalent Fellow with the High Voltage Laboratory, IIT Madras. His research interests include condition monitoring and design of suitable nanocomposite insulation systems for power apparatus.

RAMANUJAM SARATHI (Senior Member, IEEE) received the Ph.D. degree in high voltage engineering from the Indian Institute of Science, Bangalore, India, in 1994.

He is currently a Professor and the Head of the High Voltage Laboratory, Department of Electrical Engineering, IIT Madras, Chennai, India. His research interests include condition monitoring of power apparatuses and nanomaterials.

STEFAN KORNHUBER received the Diploma degree in electrical power engineering and the Ph.D. degree in temperature measurement and uprating of overhead transmission lines from the Graz University of Technology, Graz, Austria, in 2005 and 2007, respectively.

His research interests include the outer and inner electrical interfaces of polymeric materials and the diagnosis. He is a member of different working groups at CIGRE, IEC, and DKE, and is a Convener of CIGRE D1.58 and IEC TC 112 WG3. He was a recipient of the Professorship in High Voltage Engineering and Theoretical Electrical Engineering at the University of Applied Science Zittau/Goerlitz, in October 2014.

NARESH CHILLU (Member, IEEE) received the Ph.D. degree in automation and high voltage engineering from IIT Madras, Chennai, India, in 2021.

He is currently working as an Assistant Professor with the School of Electronics Engineering (SENSE), VIT AP University. His research interests include automation and preparation of nanocomposite materials for insulation, and EMI shielding applications.